Available online at www.sciencedirect.com

ScienceDirect

International Journal of Machine Tools & Manufacture 47 (2007) 1978–1987

INTERNATIONAL JOURNAL OF MACHINE TOOLS & MANUFACTURE DESIGN, RESEARCH AND APPLICATION

www.elsevier.com/locate/ijmactool

A novel simple and low cost 4 degree of freedom angular indexing calibrating technique for a precision rotary table

W. Jywe[a,*], C.J. Chen[b], W.H. Hsieh[a], P.D. Lin[b], H.H. Jwo[a], T.Y. Yang[a]

[a]National Formosa University, Department of Automation Engineering, No. 64 Wenhua Rd., Huwei, Taiwan, ROC
[b]National Cheng-Kung University, Department of Mechanical Engineering, No. 1, University Rd., Tainan, Taiwan, ROC

Received 30 October 2006; received in revised form 1 February 2007; accepted 13 February 2007
Available online 25 February 2007

Abstract

For calibrating an angular rotary table, either a high precision standard table or a laser interferometer and related optics are normally employed at high cost. This paper establishes a novel, simple and low cost technique to calibrate the 4-degrees-of-freedom (DOF) errors of a rotary table (three angular position errors and one linear position error) for a 360° full circle by employing one reference rotary table, one 1 dimensional (1D) grating and two 2 dimensional (2D) position-sensing-detectors (PSD). With this technique, no highly accurate reference rotary table, but with good repeatability is needed. After two full circle tests, the 4-DOF errors of both the target rotary table and the reference rotary table could be obtained. The system calibration, stability test, system verification and full circle test were completed. The angular stability of this system was less then 2 arc sec, while the displacement stability was less than 1.2 μm.

Keywords: Rotary table calibration; Full circle test; Grating; Position sensing detector; 4 Degree of freedom measurement; Error separation

1. Introduction

A rotary table is frequently used in industry in such things as machine tools, CMM and assembly lines. Therefore, the calibration of the rotary table is very important. The calibration of the rotary table requires an angle measurement instrument, and the conventional instruments are the rotary encoder, the laser interferometer, the autocollimator and the precision level. A rotary encoder [1] is commonly used in indexing measurement in a rotary machine, e.g. a rotary table of the multi-axis machine tool, the joint of a robot, the spindles of machine tools and the indexing of a ball screw. However, the rotary encoder is only suitable for the indexing error measurement. A laser interferometer [2] has often been used to measure a small angle, but it can only obtain indexing error during an indexing test. An autocollimator [3] is frequently used to measure small angles and it can be applied to two dimensional (2D) angle measurement (pitch error and yaw error), but its measurement range is small and it require one standard polygon mirror. A rotary table has 6 DOF errors (3 linear position errors and 3 angular position errors), but conventional instruments can only measure either one dimensional (1D) error or 2D errors. The complete calibration procedure of a rotary table requires 6 DOF measurement for a 360° full circle, but the measurement range of most measurement systems is smaller than 10°. Therefore the measurement range of the laser interferometer and autocollimator are not enough and, in addition, they are expensive. The conventional calibration technique of the rotary table for a 360° full circle requires one reference rotary table, which must have high accuracy and high repeatability. The error of the reference rotary table could then be ignored from the measurement results. The instrument usually recorded one time when the target rotary table was rotated clockwise and the reference rotary table was rotated counterclockwise. In general, one rotary table calibration for a 360° full circle requires 36 recording if the sampled period of measurement system is 10°. If a

*Corresponding author. National Formosa University, Department of Automation Engineering, No. 64 Wenhua Rd., Huwei, Taiwan, ROC. Tel.: +886 56315402; fax: +886 56311500.

E-mail addresses: jywe@sunws.nfu.edu.tw (W. Jywe), pmc2@sunws.nfu.edu.tw (C.J. Chen), allen@nfu.edu.tw (W.H. Hsieh), pdlin@mail.ncku.edu.tw (P.D. Lin), schong@nfu.edu.tw (H.H. Jwo), jeyang@ms61.hinet.net (T.Y. Yang).

0890-6955/$ - see front matter
doi:10.1016/j.ijmachtools.2007.02.004

more complete test is implemented, the calibration process will takes a long time.

In general, the rotary table includes the index error, wobble error and eccentricity. But conventional rotary table calibration techniques (laser interferometer or autocollimator) only calibrate the index error and the wobble error. However, the high precision rotary table must be calibrated in more details. Through the complete rotary table calibration, the errors of rotary table can be compensated. In this paper, the errors of rotary table were defined by 6 DOF, i.e. three linear position errors (δ_x, δ_y, δ_z) and three angular position errors (ε_x, ε_y, ε_z). The index error was represented by ε_z, the wobble error was represented by ε_x and ε_y, the eccentricity was represented by δ_x and δ_y.

In recent years, angular measuring techniques have focused on the interferometric methods. In 1992, Huang et al. [4] developed a small angle measurement system which was based on the internal reflection effect in a glass boundary and Fresnel's law. In Huang's system, the resolution was 0.2 arc sec and the measuring range was 3 arc sec. In 1996, Xiaoli et al. [5] established a 2D small rotation angle-measurement system using two different parallel interference patterns (PIP) that were orthogonal to each other. The standard deviation of Xiaoli's system was 0.6 arc sec. In the following year Xiaoli et al. [6] improved their system so that its resolution was 0.2 arc sec and measuring range was ± 30 arc min. In 1997, Chiu et al. [7] established a modified angle measurement technique with a resolution of 0.333 arc sec and a measuring range of $\pm 5.6°$. At its optimum performance, the system's resolution was 0.288 arc sec. In 1998, Zhou and Cai [8] established an angle measurement technique which was based on the total-internal reflection effect and heterodyne interferometry. The system resolution was better than 0.3 arc sec, depending on the refractive index selected. In 1998, Huang et al. [9] established a method of angle measurement, based on the internal reflection effects, that used a single right-angle prism. They demonstrated that angle measurement with a range of ± 500 arc min, a nonlinearity error of $\pm 0.1\%$, and a resolution of 0.1 arc sec could be readily achieved. In 1999, Guo et al. [10] developed an optical method for small angle measurement based on surface-plasma resonance (SPR), and a measurement resolution of 0.2 arc sec was achieved experimentally. In 2003, Ge and Makeda [11] developed an angle-measurement technique based on fringe analysis for phase-measuring profilometry. The measurement range was ± 2160 arc sec and the deviation from linearity was better than ± 0.02 arc sec. In 2004, Chiu et al. [12] developed an instrument for measuring small angles using multiple total internal reflections in heterodyne interferometry, and the angular resolution was better than 0.454 arc sec over the measurement range $-2.12° \leqslant \theta \leqslant 2.12°$ for 20 total-internal reflections.

Most angle-measurement technique research focuses on 1D angle measurement and interferometric angle measurement, and 2D measurement also focuses on interferometric techniques. However, interferometric systems are expensive and complex, and cannot be used extensively in industry. Therefore, the low cost and multiple DOF measurement system is needed for rotary table calibration. The position sensing detector (PSD) could be used to measure the rotary part error, the speed of rotary part, the rotation direction of rotary part, the angular position, and the indexing error [13,14]. Jywe et al. employed two PSDs and one reflective grating to test rotary table performance [15], but its measurement range was small ($<1°$). In [15], no full circle test was implemented and no analytic solution was provided. However, for the general rotary table calibration, the 360° full circle test is necessary. This paper both describes the building of one 4-DOF measurement system and establishes a novel technique for rotary table full circle test. The 4-DOF system presented in this paper comprises one 1D reflection grating, one laser diode, four PSDs and one reference rotary table.

The laser interferometer and the autocollimator were most used rotary table measurement system. However, in rotary table calibration process, the laser interferometer and the autocollimator need a high accuracy reference rotary table and a polygon mirror, respectively. Therefore, using the laser interferometer or autocollimator to calibrate rotary table is expensive. Because , the cost of 1D reflection grating, PSD, signal conditioning unit of PSD and laser diode and rotary table is about $\frac{1}{5}$ of one laser interferometer system or $\frac{1}{2}$ of one autocollimator system. Moreover, in the presented method, no high accurate reference rotary table, but with good repeatability is needed. Even the indexing error and the geometric error of the reference rotary table is large, they will be obtained by the presented method.

2. The 4-DOF measurement system

In this paper, the 4-DOF measurement system includes one reference rotary table, one 1D grating, one laser diode, two PSDs, two PSD processors, one A/D card and one personal computer (PC). Fig. 1 shows the schematic diagram. The reference rotary table was placed on the target rotary table then the 1D grating was mounted on the rotary table by the fixture. The laser diode and PSDs were placed near the 1D grating. The laser beam from the laser diode was projected onto a 1D grating and then the 1D grating produced many diffraction light beams. In this paper, the +1 order and −1 order diffraction light beam are used, and two PSDs were used to detect the diffraction light beam. Generally six geometric errors are defined on a rotary table, namely three linear position errors and three angular position errors (pitch, roll, and yaw). The three linear position errors are δ_x, δ_y and δ_z, and the three angular position errors are ε_x, ε_y and ε_z, respectively. In addition, there are eccentricity between the grating and the axis of the rotary table, which are defined as D_x and D_y. The distance from the light point on the grating to the rotary table origin point is h_0.

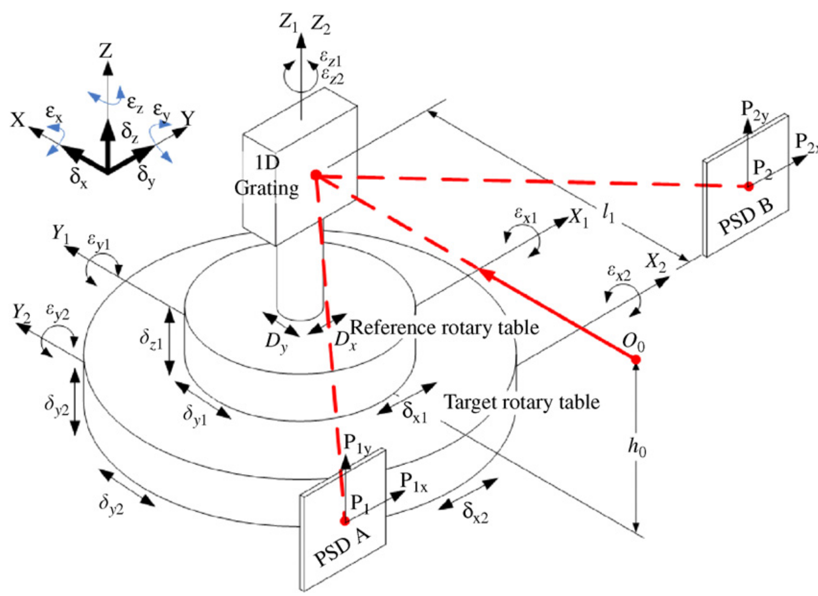

Fig. 1. The schematic diagram of the 4-DOF measurement system.

The outputs of PSDs were effect by the D_y, δ_y, ε_x, ε_y and ε_z. Therefore, the PSD A x-axis output is

$$\begin{aligned} P_{Ax} &= l_1[\sin(\theta + 2\varepsilon_z) - \sin\theta] + (D_y + \delta_y)\tan\theta \\ &= l_1[\sin\theta\cos 2\varepsilon_z + \cos\theta\sin 2\varepsilon_z - \sin\theta] \\ &\quad + (D_y + \delta_y)\tan\theta, \end{aligned} \tag{1}$$

where θ is the diffraction angle of the grating, l_1 is the distance between the PSD and the grating. The diffraction equation of the grating is

$$n\lambda = d(\sin\theta \pm \sin\theta'), \tag{2}$$

where n is the order of diffraction, d is the grating constant, λ is the wavelength of the laser source, θ' is the incident angle and θ is the diffraction angle. In this paper, d is $1/600$ mm, $\lambda = 650$ nm and $n = 1$. Therefore, the diffraction angle θ is $22.954°$.

The PSD A y-axis output is

$$P_{Ay} = (h_0 \sin\varepsilon_x + l_1)\tan 2\varepsilon_x + (l_1 \sin\theta + h_0 \sin\varepsilon_y)\tan\varepsilon_y. \tag{3}$$

The PSD B x-axis output is

$$\begin{aligned} P_{Bx} &= l_1[\sin\theta - \sin(\theta - 2\varepsilon_z)] - (D_y + \delta_y)\tan\theta \\ &= l_1[\sin\theta - \sin\theta\cos 2\varepsilon_z + \cos\theta\sin 2\varepsilon_z] \\ &\quad - (D_y + \delta_y)\tan\theta. \end{aligned} \tag{4}$$

The PSD B y-axis output is

$$P_{By} = (h_0 \sin\varepsilon_x + l_1)\tan 2\varepsilon_x - (l_1 \sin\theta - h_0 \sin\varepsilon_y)\tan\varepsilon_y. \tag{5}$$

From the above equations, the four geometric errors can be derived. ε_z is

$$\varepsilon_z = \frac{1}{2}\sin^{-1}\left(\frac{P_{Ax} + P_{Bx}}{2l_1\cos\theta}\right), \tag{6}$$

or

$$l_1 = \frac{P_{Ax} + P_{Bx}}{2\cos\theta\sin 2\varepsilon_z}. \tag{7}$$

From Eq. (7), the distance between the grating and PSD can be calculated, if the ε_z is known. The linear error in the y direction is

$$\begin{aligned} D_y + \delta_y &= \frac{P_{Ax} - l_1[\sin\theta\cos 2\varepsilon_z + \cos\theta\sin 2\varepsilon_z - \sin\theta]}{\tan\theta} \\ &= \frac{l_1[\sin\theta - \sin\theta\cos 2\varepsilon_z + \cos\theta\sin 2\varepsilon_z] - P_{Bx}}{\tan\theta}. \end{aligned} \tag{8}$$

In a full circle test, D_y is constant, δ_y is the function value of the rotary angle and the summation of δ_y is zero. Therefore, Eq. (8) can be rewritten as

$$\delta_y = \frac{l_1[\sin\theta - \sin\theta\cos 2\varepsilon_z + \cos\theta\sin 2\varepsilon_z] - P_{Bx}}{\tan\theta} - D_y. \tag{9}$$

From Eqs. (3) and (5), ε_y is

$$\varepsilon_y = \tan^{-1}\left(\frac{P_{Ay} - P_{By}}{2l_1\sin\theta}\right). \tag{10}$$

The summation of the PSD A y-axis and the PSD B y-axis is

$$P_{Ay} + P_{By} = 2(h_0 \sin\varepsilon_x + l_1)\tan 2\varepsilon_x + 2h_0 \sin\varepsilon_y \tan\varepsilon_y. \tag{11}$$

Because $h_0 \sin\varepsilon_x \ll l_1$, Eq. (11) can be written as

$$\varepsilon_x = \frac{1}{2}\tan^{-1}\left(\frac{P_{Ay} + P_{By} - 2h_0\sin\varepsilon_y\tan\varepsilon_y}{2l_1}\right). \tag{12}$$

From Eqs. (6), (9), (10) and (12), the δ_y, ε_x, ε_y and ε_z can be obtained throughout the PSD A and PSD B outputs.

3. The model of the full circle test

The measurement range of most instruments is less than 10°, so the complete calibration of a rotary table requires a special method. In normal rotary table calibration, the autocollimator uses one polygon mirror and the laser interferometer uses one reference rotary table. In this paper, the technique also requires one reference rotary table, but the requirement of the reference rotary table is only that the errors of reference rotary table must be repeatable. In 1994, Lin [16] established a rotary table calibration technique which could measure the indexing error of the rotary table for a 360° full circle. However, the technique could only measure the indexing error. Consequently, an improved technique is established in this section. When the errors of the reference rotary table were considered, the geometric errors of the rotary table are

$$\begin{aligned} &\varepsilon_x = \varepsilon_{xt} + \varepsilon_{xr}, \quad \delta_x = \delta_{xt} + \delta_{xr},\\ &\varepsilon_y = \varepsilon_{yt} + \varepsilon_{yr}, \quad \delta_y = \delta_{yt} + \delta_{yr},\\ &\varepsilon_z = \varepsilon_{zt} - \varepsilon_{zr}, \quad \delta_z = \delta_{zt} + \delta_{zr}, \end{aligned} \tag{13}$$

where ε_z is the index difference between the target rotary table and the reference rotary table, and it accumulatively varies during the calibration procedure. The ε_x, ε_y, δ_x, δ_y and δ_z are not accumulative. Because one full circle test needs two tests, the repeatability of the target rotary table and the reference rotary table must be good, otherwise the measured results will not repeat.

The basic requirement of the calibrating technique is that the target rotary table under calibration can be rotated the same step size as the reference rotary table in different orientations, say on for clockwise and the other counter-clockwise. Each sector of the table under test has been compared with every sector of the reference one in order to build the first set of data. For example, one rotary table was tested at 12 angular position points around 360° (i.e. at $0^\circ,30^\circ,60^\circ,\ldots,330^\circ$), which were equally spaced segmented in the target rotary table and the reference rotary table. At the start in the first test, after the target rotary table and reference rotary table were set at 0° the first set of sample was taken by personal computer. Then, the target rotary table was rotated 30° clockwise and the reference rotary table was rotated 30° counter-clockwise and the other sets of sample were taken by personal computer. From the above experiment process, the following relationship can be derived:

$$\begin{aligned} &\varepsilon_{z11} = \varepsilon_{zt1} - \varepsilon_{zr1},\\ &\varepsilon_{z12} = \varepsilon_{zt2} - \varepsilon_{zr2},\\ &\vdots\\ &\varepsilon_{z1n} = \varepsilon_{ztn} - \varepsilon_{zrn}, \end{aligned} \tag{14}$$

where ε_{z1n} is the first set of angular readings and n is the number of increments over 360°. The subscript 't' of the symbol ε_{zt1} means the error of the target rotary table and the subscript 'r' means the error of the reference rotary table.

In the second test of full circle test, the target rotary table and reference rotary table was set to 0° again and the reference rotary table was incremented by one nominal step (ex. 30°). After the rotation of the reference rotary table, the first set of sample was taken. Then, the target rotary table was rotated 30° clockwise and the reference rotary table was rotated 30° counter-clockwise and the other sets of sample were taken. From the above experiment process, the results of second test were obtained. Then, the flowing relationship can be derived:

$$\begin{aligned} &\varepsilon_{z21} = \varepsilon_{zt1} - \varepsilon_{zr2},\\ &\varepsilon_{z22} = \varepsilon_{zt2} - \varepsilon_{zr3},\\ &\vdots\\ &\varepsilon_{z2n} = \varepsilon_{ztn} - \varepsilon_{zr1}, \end{aligned} \tag{15}$$

where ε_{z2n} is the second set of angular readings and n is the number of increments over 360°. The two sets of measured data can then be rearranged as follows:

$$\begin{bmatrix} 1 & 0 & 0 & 0 & \cdots & -1 & 0 & 0 & 0 & 0 & \cdots & 0\\ 0 & 1 & 0 & 0 & \cdots & 0 & -1 & 0 & 0 & 0 & \cdots & 0\\ 0 & 0 & 1 & 0 & \cdots & 0 & 0 & -1 & 0 & 0 & \cdots & 0\\ \vdots & \vdots & \vdots & \vdots & & \vdots & \vdots & \vdots & \vdots & \vdots & & \vdots\\ 1 & 0 & 0 & 0 & \cdots & 0 & -1 & 0 & 0 & 0 & \cdots & 0\\ 0 & 1 & 0 & 0 & \cdots & 0 & 0 & -1 & 0 & 0 & \cdots & 0\\ 0 & 0 & 1 & 0 & \cdots & 0 & 0 & 0 & -1 & 0 & \cdots & 0\\ \vdots & \vdots & \vdots & \vdots & & \vdots & \vdots & \vdots & \vdots & \vdots & & \vdots\\ 0 & 0 & 0 & 0 & \cdots 1 & -1 & 0 & 0 & 0 & 0 & \cdots & 0 \end{bmatrix} \begin{bmatrix} \varepsilon_{zt1}\\ \varepsilon_{zt2}\\ \varepsilon_{zt3}\\ \vdots\\ \varepsilon_{zr1}\\ \varepsilon_{zr2}\\ \varepsilon_{zr3}\\ \vdots\\ \varepsilon_{zrn} \end{bmatrix} = \begin{bmatrix} \varepsilon_{z11}\\ \varepsilon_{z12}\\ \varepsilon_{z13}\\ \vdots\\ \varepsilon_{z21}\\ \varepsilon_{z22}\\ \varepsilon_{z23}\\ \vdots\\ \varepsilon_{z2n} \end{bmatrix} \tag{16}$$

and the original augmented matrix is shown as:

$$\left[\begin{array}{cccccccccccc} 1 & 0 & 0 & 0 & \cdots & -1 & 0 & 0 & 0 & 0 & \cdots & \varepsilon_{z11} \\ 0 & 1 & 0 & 0 & \cdots & 0 & -1 & 0 & 0 & 0 & \cdots & \varepsilon_{z12} \\ 0 & 0 & 1 & 0 & \cdots & 0 & 0 & -1 & 0 & 0 & \cdots & \varepsilon_{z13} \\ \vdots & \vdots & \vdots & \vdots & & \vdots & \vdots & \vdots & \vdots & \vdots & & \vdots \\ 1 & 0 & 0 & 0 & \cdots & 0 & -1 & 0 & 0 & 0 & \cdots & \varepsilon_{z21} \\ 0 & 1 & 0 & 0 & \cdots & 0 & 0 & -1 & 0 & 0 & \cdots & \varepsilon_{z22} \\ 0 & 0 & 1 & 0 & \cdots & 0 & 0 & 0 & -1 & 0 & \cdots & \varepsilon_{z23} \\ \vdots & \vdots & \vdots & \vdots & & \vdots & \vdots & \vdots & \vdots & \vdots & & \vdots \\ 0 & 0 & 0 & 0 & \cdots 1 & -1 & 0 & 0 & 0 & 0 & \cdots & \varepsilon_{z2n} \end{array}\right]. \tag{17}$$

An augmented matrix of the reduced system can then be derived as follows:

$$\left[\begin{array}{cccccccccccc} 1 & 0 & 0 & 0 & \cdots & -1 & 0 & 0 & 0 & 0 & \cdots & 0 & \varepsilon_{z11} \\ 0 & 1 & 0 & 0 & \cdots & 0 & -1 & 0 & 0 & 0 & \cdots & 0 & \varepsilon_{z12} \\ 0 & 0 & 1 & 0 & \cdots & 0 & 0 & -1 & 0 & 0 & \cdots & 0 & \varepsilon_{z13} \\ \vdots & \vdots & \vdots & \vdots & & \vdots & \vdots & \vdots & \vdots & \vdots & & \vdots & \vdots \\ 0 & 0 & 0 & 0 & \cdots & 1 & -1 & 0 & 0 & 0 & \cdots & 0 & \varepsilon_{z21}-\varepsilon_{z11} \\ 0 & 0 & 0 & 0 & \cdots & 0 & 1 & -1 & 0 & 0 & \cdots & 0 & \varepsilon_{z22}-\varepsilon_{z12} \\ 0 & 0 & 0 & 0 & \cdots & 0 & 0 & 1 & -1 & 0 & \cdots & 0 & \varepsilon_{z23}-\varepsilon_{z13} \\ \vdots & \vdots & \vdots & \vdots & & \vdots & \vdots & \vdots & \vdots & \vdots & & \vdots & \vdots \\ 0 & 0 & 0 & 0 & \cdots & 1 & 0 & 0 & 0 & 0 & \cdots & -1 & \sum_{i=1}^{n-1}(\varepsilon_{z2i}-\varepsilon_{z1i}) \\ 0 & 0 & 0 & 0 & \cdots & -1 & 0 & 0 & 0 & 0 & \cdots & 1 & \varepsilon_{z2n}-\varepsilon_{z1n} \end{array}\right]. \tag{18}$$

From the last two rows in the reduced matrix, it can be shown that

$$\varepsilon_{zr1}-\varepsilon_{zrn}=\sum_{i=1}^{n-1}(\varepsilon_{z2i}-\varepsilon_{z1i})=-(\varepsilon_{z2n}-\varepsilon_{z1n}), \tag{19}$$

or

$$\sum_{i=1}^{n-1}(\varepsilon_{z2i}-\varepsilon_{z1i})=0.$$

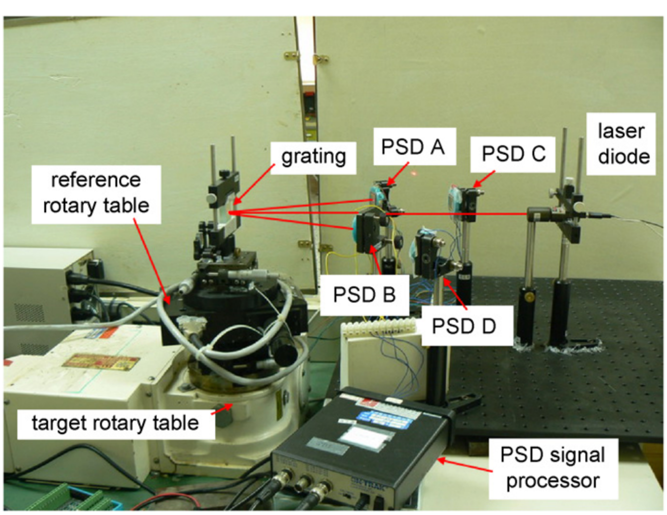

Fig. 2. Photograph of the 4DOF measurement system with 4 PSD.

Since Eq. (18) is linear-dependent, more equations are required. An assumption is again made to presume that no closing error exists within the reference rotary table and consequently the following equation can be derived:

$$\varepsilon_{zr1}+\varepsilon_{zr2}+\varepsilon_{zr3}+\cdots+\varepsilon_{zrn-1}+\varepsilon_{zrn}=360^\circ. \tag{20}$$

Table 1
Components of the prototype 4-DOF measurement system

PSD	UDT SC-10D, active area 100 mm^2
PSD signal processor	On-Trak OT-301
PC	Intel Pentium4 2.0 G 256 MB RAM 40 G HD
A/D Card	Advantech PCI-1716, 16 bit, sampling range ± 10 V, Max. sampling frequency 250 kHz
Laser diode	$\lambda = 635$ nm, 5 mW
1D Grating	Rolled diffraction grating, 600 grooves per mm,
Autocollimator	NewPort LDS Vector, measurement range: 2000 μrad

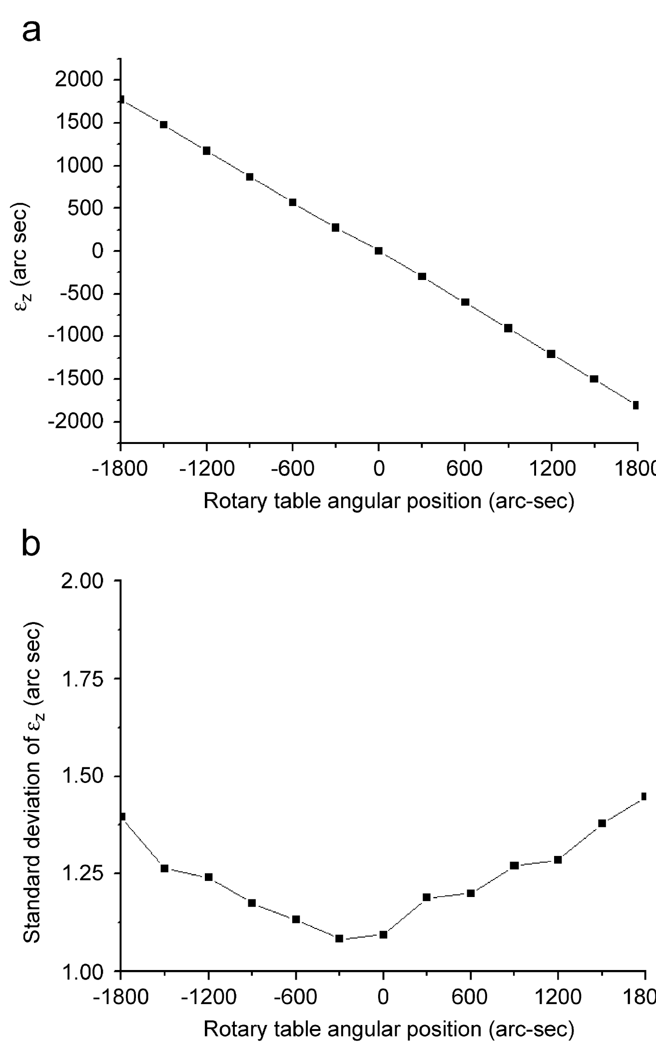

Fig. 3. Calibration results (b) standard deviation.

Eq. (20) is then incorporated into the augmented matrix in Eq. (18) to give the following:

$$\left[\begin{array}{cccccccccccc|c}
1 & 0 & 0 & 0 & \cdots & -1 & 0 & 0 & 0 & 0 & \cdots & 0 & \varepsilon_{z11} \\
0 & 1 & 0 & 0 & \cdots & 0 & -1 & 0 & 0 & 0 & \cdots & 0 & \varepsilon_{z12} \\
0 & 0 & 1 & 0 & \cdots & 0 & 0 & -1 & 0 & 0 & \cdots & 0 & \varepsilon_{z13} \\
\vdots & \vdots & \vdots & \vdots & & \vdots & \vdots & \vdots & \vdots & \vdots & & \vdots & \vdots \\
1 & 0 & 0 & 0 & \cdots & 0 & -1 & 0 & 0 & 0 & \cdots & 0 & \varepsilon_{z21} \\
0 & 1 & 0 & 0 & \cdots & 0 & 0 & -1 & 0 & 0 & \cdots & 0 & \varepsilon_{z22} \\
0 & 0 & 1 & 0 & \cdots & 0 & 0 & 0 & -1 & 0 & \cdots & 0 & \varepsilon_{z23} \\
\vdots & \vdots & \vdots & \vdots & & \vdots & \vdots & \vdots & \vdots & \vdots & & \vdots & \vdots \\
0 & 0 & 0 & 0 & \cdots 1 & -1 & 0 & 0 & 0 & 0 & \cdots & 0 & \varepsilon_{z2n} \\
0 & 0 & 0 & 0 & \cdots 0 & 1 & 1 & 1 & 1 & 1 & \cdots & 1 & 360
\end{array}\right]. \tag{21}$$

Finally, using the Gaussian Elimination method, the actual individual angle ε_{zti} and ε_{zri} at each target position can be calculated. The calculation of ε_{xti}, ε_{xri}, ε_{yti}, ε_{yri}, δ_{xti}, δ_{xri}, δ_{yti}, δ_{yri}, δ_{zti} and δ_{zri} is different to ε_{zti} and ε_{zri}. For instance,

$$\begin{aligned}
\varepsilon_{x11} &= \varepsilon_{xt1} + \varepsilon_{xr1}, \\
\varepsilon_{x12} &= \varepsilon_{xt2} + \varepsilon_{xr2}, \\
&\vdots \\
\varepsilon_{x1n} &= \varepsilon_{xtn} + \varepsilon_{xrn}
\end{aligned} \tag{22}$$

and

$$\begin{aligned}
\varepsilon_{x21} &= \varepsilon_{xt1} - \varepsilon_{xr2}, \\
\varepsilon_{x22} &= \varepsilon_{xt2} - \varepsilon_{xr3}, \\
&\vdots \\
\varepsilon_{x2n} &= \varepsilon_{xtn} - \varepsilon_{xr1}.
\end{aligned} \tag{23}$$

The summation of ε_{xri} is

$$\varepsilon_{xr1} + \varepsilon_{xr2} + \varepsilon_{xr3} + \cdots + \varepsilon_{xrn-1} + \varepsilon_{xrn} = 0^\circ. \tag{24}$$

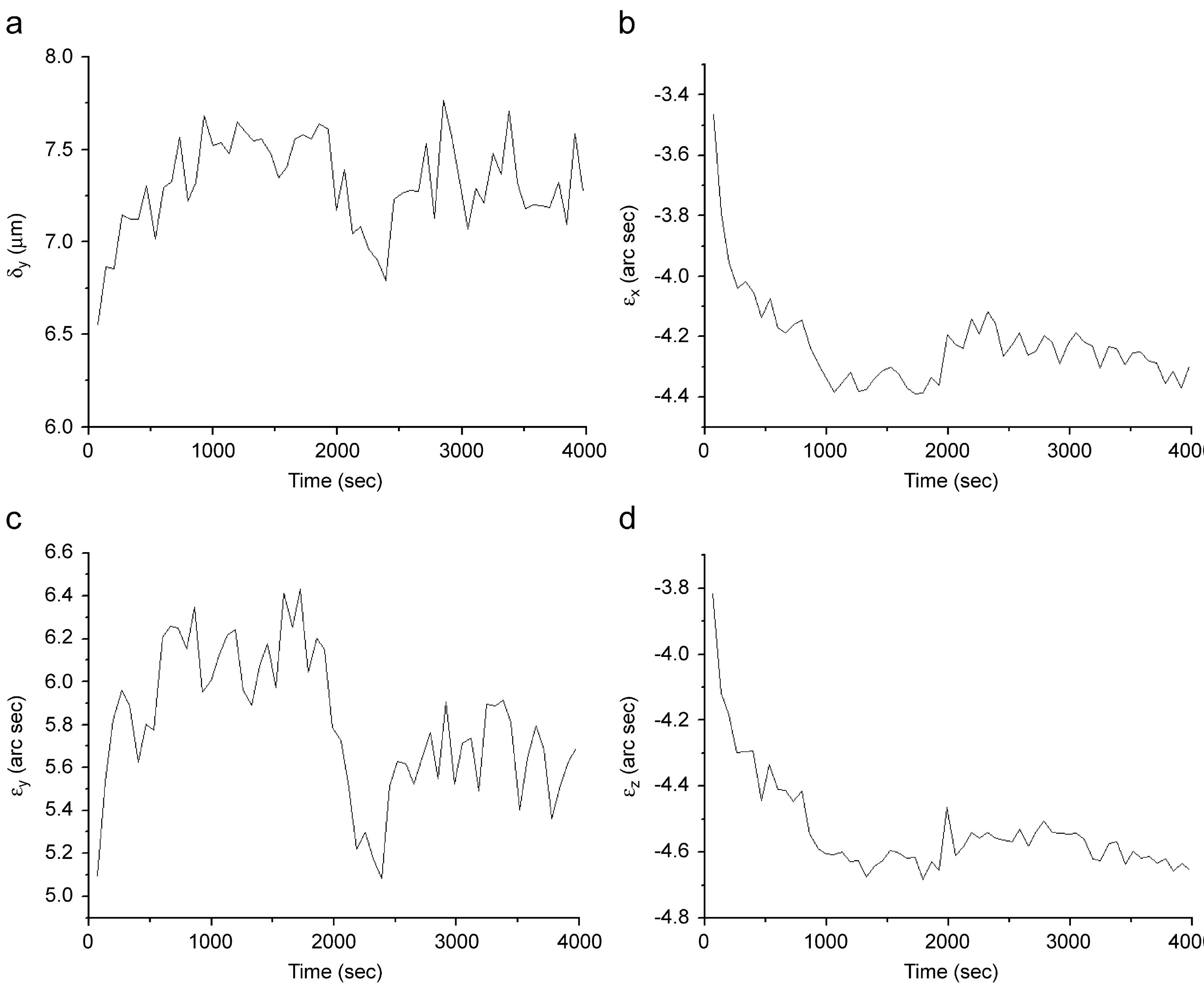

Fig. 4. Stability test results (a)–(d).

Therefore, the matrix of ε_{xti} and ε_{xri} is

$$\begin{bmatrix} 1 & 0 & 0 & 0 & \cdots & -1 & 0 & 0 & 0 & 0 & \cdots & 0 & \varepsilon_{x11} \\ 0 & 1 & 0 & 0 & \cdots & 0 & -1 & 0 & 0 & 0 & \cdots & 0 & \varepsilon_{x12} \\ 0 & 0 & 1 & 0 & \cdots & 0 & 0 & -1 & 0 & 0 & \cdots & 0 & \varepsilon_{x13} \\ \vdots & \vdots & \vdots & \vdots & & \vdots & \vdots & \vdots & \vdots & \vdots & & \vdots & \vdots \\ 1 & 0 & 0 & 0 & \cdots & 0 & -1 & 0 & 0 & 0 & \cdots & 0 & \varepsilon_{x21} \\ 0 & 1 & 0 & 0 & \cdots & 0 & 0 & -1 & 0 & 0 & \cdots & 0 & \varepsilon_{x22} \\ 0 & 0 & 1 & 0 & \cdots & 0 & 0 & 0 & -1 & 0 & \cdots & 0 & \varepsilon_{x23} \\ \vdots & \vdots & \vdots & \vdots & & \vdots & \vdots & \vdots & \vdots & \vdots & & \vdots & \vdots \\ 0 & 0 & 0 & 0 & \cdots 1 & -1 & 0 & 0 & 0 & 0 & \cdots & 0 & \varepsilon_{x2n} \\ 0 & 0 & 0 & 0 & \cdots 0 & 1 & 1 & 1 & 1 & 1 & \cdots & 1 & 0 \end{bmatrix}. \tag{25}$$

Similarly,

$$\begin{bmatrix} 1 & 0 & 0 & 0 & \cdots & -1 & 0 & 0 & 0 & 0 & \cdots & 0 & \varepsilon_{y11} \\ 0 & 1 & 0 & 0 & \cdots & 0 & -1 & 0 & 0 & 0 & \cdots & 0 & \varepsilon_{y12} \\ 0 & 0 & 1 & 0 & \cdots & 0 & 0 & -1 & 0 & 0 & \cdots & 0 & \varepsilon_{y13} \\ \vdots & \vdots & \vdots & \vdots & & \vdots & \vdots & \vdots & \vdots & \vdots & & \vdots & \vdots \\ 1 & 0 & 0 & 0 & \cdots & 0 & -1 & 0 & 0 & 0 & \cdots & 0 & \varepsilon_{y21} \\ 0 & 1 & 0 & 0 & \cdots & 0 & 0 & -1 & 0 & 0 & \cdots & 0 & \varepsilon_{y22} \\ 0 & 0 & 1 & 0 & \cdots & 0 & 0 & 0 & -1 & 0 & \cdots & 0 & \varepsilon_{y23} \\ \vdots & \vdots & \vdots & \vdots & & \vdots & \vdots & \vdots & \vdots & \vdots & & \vdots & \vdots \\ 0 & 0 & 0 & 0 & \cdots 1 & -1 & 0 & 0 & 0 & 0 & \cdots & 0 & \varepsilon_{y2n} \\ 0 & 0 & 0 & 0 & \cdots 0 & 1 & 1 & 1 & 1 & 1 & \cdots & 1 & 0 \end{bmatrix}, \tag{26}$$

$$\begin{bmatrix} 1 & 0 & 0 & 0 & \cdots & -1 & 0 & 0 & 0 & 0 & \cdots & 0 & \delta_{y11} \\ 0 & 1 & 0 & 0 & \cdots & 0 & -1 & 0 & 0 & 0 & \cdots & 0 & \delta_{y12} \\ 0 & 0 & 1 & 0 & \cdots & 0 & 0 & -1 & 0 & 0 & \cdots & 0 & \delta_{y13} \\ \vdots & \vdots & \vdots & \vdots & & \vdots & \vdots & \vdots & \vdots & \vdots & & \vdots & \vdots \\ 1 & 0 & 0 & 0 & \cdots & 0 & -1 & 0 & 0 & 0 & \cdots & 0 & \delta_{y21} \\ 0 & 1 & 0 & 0 & \cdots & 0 & 0 & -1 & 0 & 0 & \cdots & 0 & \delta_{y22} \\ 0 & 0 & 1 & 0 & \cdots & 0 & 0 & 0 & -1 & 0 & \cdots & 0 & \delta_{y23} \\ \vdots & \vdots & \vdots & \vdots & & \vdots & \vdots & \vdots & \vdots & \vdots & & \vdots & \vdots \\ 0 & 0 & 0 & 0 & \cdots 1 & -1 & 0 & 0 & 0 & 0 & \cdots & 0 & \delta_{y2n} \\ 0 & 0 & 0 & 0 & \cdots 0 & 1 & 1 & 1 & 1 & 1 & \cdots & 1 & 0 \end{bmatrix}. \tag{27}$$

This technique can be used in the rotary table 6-DOF calibration, but in this paper, the measurement system could only measure 4-DOF errors, so this paper lists only four equations (Eqs. (21), (25)–(27)).

The recorded count was based on the measurement range of the system. For example, the measurement range of Lin's system (laser interferometer) [16] was about 10°. Therefore, one full circle test must record at least 36 points during the first and second tests, respectively.

4. Experimental results and discussion

In this paper, the calibration of the 4-DOF measurement system, system stability, system verification and full circle test were accomplished. The photograph of this system was shown in Fig. 2. Components not shown in Fig. 2 include a desktop PC connected to the PSD signal processor via an A/D card. The component specifications were listed in Table 1.

4.1. System calibration

System calibration was the first experiment. In this experiment, the NewPort autocollimator was used to provide the reference angular position. Its measurement range was ±410 arc sec, resolution was 0.02 arc sec and accuracy was 0.5 arc sec. Fig. 3(a) shows the calibration result and Fig. 3(b) gives the standard deviations for

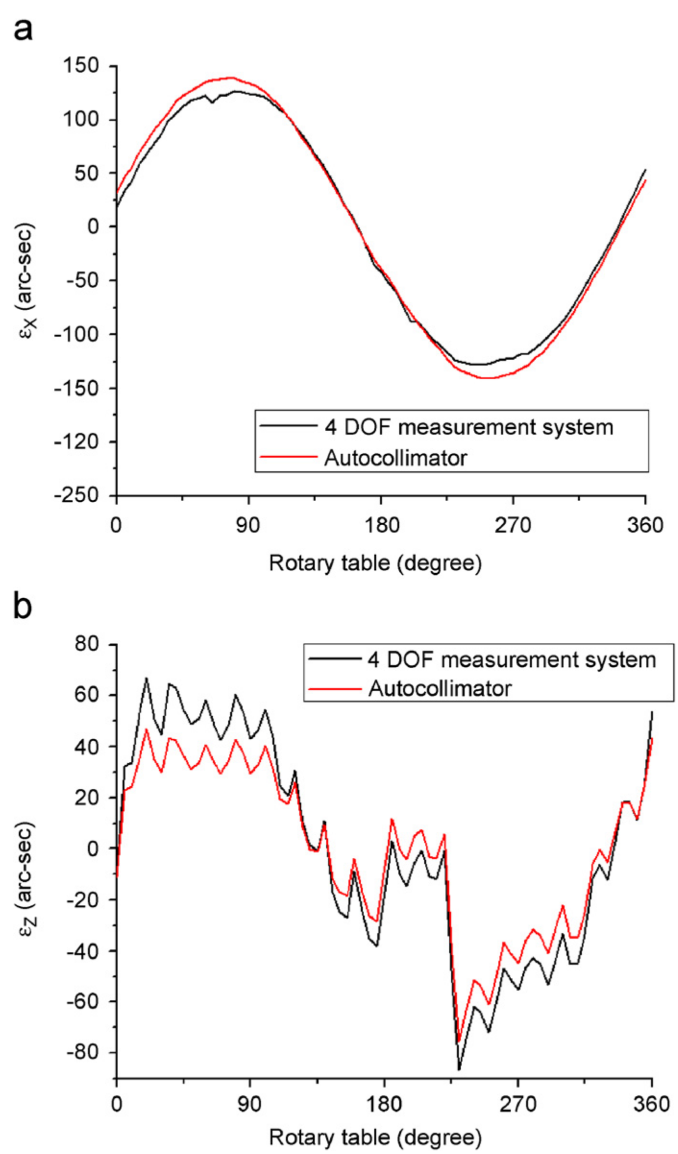

Fig. 5. Verification result (a) and (b).

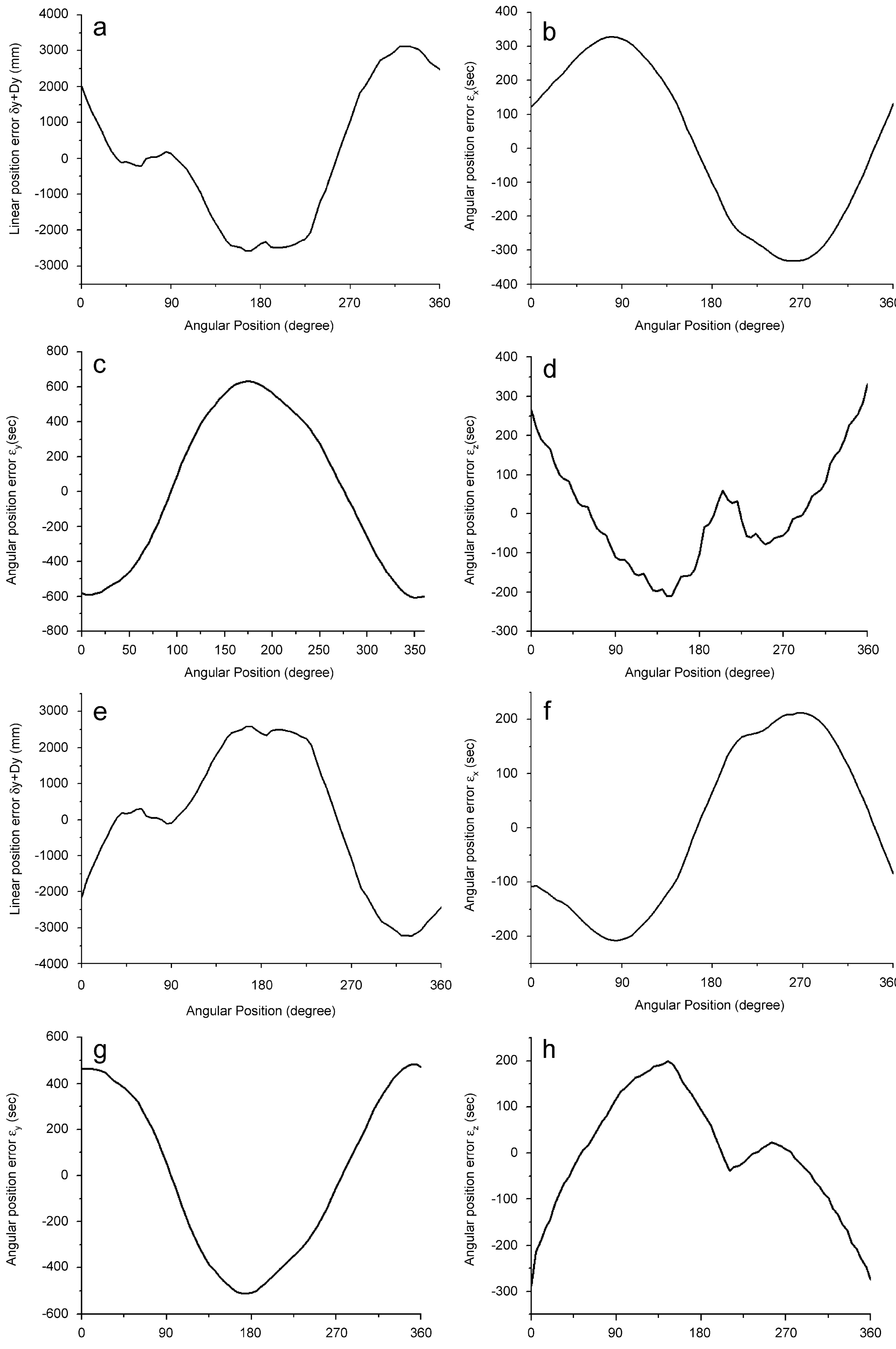

Fig. 6. Full circle test results (a)–(h).

system uncertainty. Throughout the calibration process, it was clear that the linearity of ε_z was good and the uncertainty of ε_z was about 1.5 arc sec. The angular position (ε_z) measurement range of the 4-DOF measurement system was about 1° because almost all measurement range of PSD was used.

4.2. System stability test

System stability test was the second experiment. System stability was evaluated by allowing the system to come to equilibrium under normal laboratory conditions (i.e. no special temperature or vibrational isolation) and then continuously recording the output signal for 4000 s. Fig. 4 shows that the system stability of the basic prototype was reasonable, i.e. with no special isolation or filtering the output of δ_y remained within $\pm 1.2\,\mu$m, and ε_x, ε_y and ε_z remained within ± 1.5 arc sec over 4000 s.

4.3. System verification

System verification was the third experiment, and the autocollimator was also used to verify the 4DOF measurement system, since it can measure the ε_x and ε_z simultaneously. The autocollimator was set up at the back of the grating. When the full circle test was implemented and error separation method was not used, the autocollimator recorded the error sum of the target rotary table and reference rotary table. The autocollimator and the 4DOF measurement system recorded once when the target rotary table rotated one degree clockwise and once again when the reference rotary table rotated one degree counterclockwise. Fig. 5 shows the result of the system verification. The result of 4DOF measurement system and autocollimator was similar, so the mathematic model of 4DOF measurement system is correct.

4.4. Full circle test

The full circle test was the last experiment that was described in Section 3. The measurement range of the 4-DOF measurement system is about 1°. To complete one full circle test much time must be taken if only one set PSD (2 PSD) was used. With only one set PSD requires recording at least 720 points during the first and second tests. Therefore, 4 PSDs were employed to establish the system. The PSD A and PSD B were set to sense the ± 1 order diffraction light when the angular position of the reference rotary table was at 0°. Then the PSD C and PSD D were set to sense the ± 1 order diffraction light when the angular position of the reference rotary table was set at 5°. During the full circle test, the PSD A and PSD B were employed in the first test, while PSD C and PSD D were employed in the second test. Consequently, one full circle test only requires recording 72 points during the first and second tests.

After two tests were completed, the method described above in Section 3 was used to separate the errors of the target rotary table and the reference rotary table. The test results are shown as Fig. 6(a)–(d) and (f)–(h) were the errors of target rotary table and the reference rotary table, respectively. The angular position errors of the reference rotary table were smaller than those of the target rotary table. But the indexing error is similar. δ_y, ε_x, ε_y and ε_z of the target rotary table were about 2.85 mm, 330, 620 and 270 arc sec, respectively. The δ_y, ε_x, ε_y and ε_z of the reference rotary table were about, 2.90 mm, 210, 500 and 250 arc sec, respectively.

The δ_y is large because the eccentricity between the surface of reflection grating and the central axis of rotary table is large. To adjust the eccentricity between the target rotary table and reference rotary table is easy. But to adjust eccentricity between the grating and rotary table is difficult, because the geometric for the grating and rotary table is different.

5. Conclusion

This paper established a novel, simple and low cost technique to calibrate the 4-DOF errors of a rotary table (three angular position errors and one linear position error) for a 360° full circle. With this technique, no highly accurate reference rotary table, but with good repeatability is needed. After full circle test, the 4-DOF errors of the target rotary table and the reference rotary table could be determined. The system calibration, stability test, system verification and full circle test were completed. From the system calibration, the angular uncertainty (ε_z) of the measurement system was less than 1.5 arc sec. The angular stability of this system was less then 2 arc sec, while the displacement stability was less than 1.2 μm.

Acknowledgement

Grateful appreciation is given to the National Science Council of Taiwan for financial support under Grant numbers (NSC93-2622-E-150-016- CC3), (NSC93-2212-E150-004), and (NSC94-22 12-E150-007).

References

[1] Angle Encoder, Heidenhain GmbH, 2004.
[2] Agilent 5529A Dynamic Calibrator, Agilent Technologies, 2000.
[3] LDS Electronic Autocollimator, NewPort Corporation, 1998.
[4] P.S. Huang, S. Kiyono, O. Kamada, Angle measurement based on the internal-reflection effect: a new method, Applied Optics 31 (28) (1992) 6047–6055.
[5] D. Xiaoli, S. Osami, E.G. John, S. Takamasa, Measurement of two- dimensional small rotation angles by using orthogonal parallel interference pattern, Applied Optics 35 (28) (1996) 5657–5666.
[6] D. Xiaoli, S. Osami, E.G. John, S. Takamasa, High accuracy, wide range, rotation angle measurement by the use of two parallel interference pattern, Applied Optics 36 (25) (1997) 6190–6195.
[7] M.H. Chiu, D.C. Su, Improved technique for measuring small angle, Applied Optics 36 (28) (1997) 7104–7106.
[8] W. Zhou, L. Cai, Interferometer for small-angle measurement based on total internal reflection, Applied Optics 37 (25) (1998) 5657–5666.
[9] P.S. Huang, Y. Li, Small-angle measurement by using of a single prism, Applied Optics 37 (28) (1998) 6636–6642.
[10] J. Guo, Z. Zhu, W. Deng, Small-angle measurement based on surface-plasma resonance and the use of magneto-optical modulation, Applied Optics 38 (31) (1999) 6550–6555.

[11] Z. Ge, M. Takeda, High-resolution two-dimensional angle measurement technique based on fringe analysis, Applied Optics 42 (34) (2003) 6859–6868.
[12] M.H. Chiu, S.F. Wang, R.S. Chang, Instrument for measuring small angle by use of multiple total internal reflection in heterodyne interferometry, Applied Optics 43 (29) (2004) 5438–5442.
[13] W.Y. Jywe, C.J. Chen, The development of a high-speed spindle measurement system using a laser diode and a quadrants sensor, International Journal of Machine Tools & Manufacture 45 (2005) 1162–1170.
[14] J.A. Kim, K.C. Kim, E.W. Bae, S. Kim, Y.K. Kwak, Six-degree-of-freedom displacement system using a diffraction grating, Review of Scientific Instruments 71 (8) (2000) 3214–3219.
[15] C.H. Liu, W.Y. Jywe, L.H. Shyu, C.J. Chen, Application of a diffraction grating and position sensitive detectors to the measurement of error motion and angular indexing of an indexing table, Precision Engineering 29 (2005) 440–448.
[16] K.Y. Lin, Application of laser interferometer to the automation calibration of angular indexing on machine tools, UMIST, Ph.D. Thesis, 1994.